

SUPERSONIC RETROPROPULSION ON ROBOTIC MARS LANDERS: SELECTED DESIGN TRADES

Aron A. Wolf^{*}, Connor Noyes[†], William Strauss[‡], Joel Benito[§],
Marcus Lobbia^{**}, John McCann^{††}, Barry Nakazono^{‡‡}, Zachary R. Putnam^{§§},
and Christopher G. Lorenz^{***}

Many concepts for future robotic Mars lander missions require landing heavier payloads than those landed to date. Mars lander architectures to date have relied on a parachute to help slow the lander; however the effectiveness of a parachute in the thin Martian atmosphere is diminished with heavier payloads unless the diameter of the parachute is increased or it is deployed at a higher Mach number, both of which are significant technical challenges. In addition the parachute can be successfully deployed only within a specific Mach number and dynamic pressure range. Targeting the entry trajectory to hit this “Mach-Q box” imposes constraints on the entry ballistic coefficient, limiting it to $\sim 150\text{-}200\text{ kg/m}^2$. Eliminating the parachute from the design requires descent engine ignition at supersonic speeds (Supersonic Retropropulsion, or SRP). SRP increases the propellant requirement, but also allows entry ballistic coefficients of $\sim 600\text{ kg/m}^2$ or more, with the consequence of significantly increased entry mass and landed payload mass.

* Guidance & Control Section, Jet Propulsion Lab, California Institute of Technology, 4800 Oak Grove Dr., Pasadena, CA. 91109

† Guidance & Control Section, Jet Propulsion Lab, California Institute of Technology, 4800 Oak Grove Dr., Pasadena, CA. 91109

‡ Guidance & Control Section, Jet Propulsion Lab, California Institute of Technology, 4800 Oak Grove Dr., Pasadena, CA. 91109

§ Guidance & Control Section, Jet Propulsion Lab, California Institute of Technology, 4800 Oak Grove Dr., Pasadena, CA. 91109

** Flight Systems Engineering, Integration, and Test Section; Jet Propulsion Lab; California Institute of Technology; 4800 Oak Grove Dr., Pasadena, CA. 91109

†† Spacecraft Mechanical Engineering Section, Jet Propulsion Lab, California Institute of Technology, 4800 Oak Grove Dr., Pasadena, CA. 91109

‡‡ Propulsion and Fluid Flight Systems Section, Jet Propulsion Lab, California Institute of Technology, 4800 Oak Grove Dr., Pasadena, CA. 91109

§§ Assistant Professor, Department of Aerospace Engineering, University of Illinois at Urbana-Champaign, 104 S. Wright St., Urbana, IL, 61801

*** Graduate Research Assistant, Department of Aerospace Engineering, University of Illinois at Urbana-Champaign, 104 S. Wright St., Urbana, IL, 61801

The decision to implement the SRL mission will not be finalized until NASA’s completion of the National Environmental Policy Act (NEPA) process. This document is being made available for information purposes only.

© 2018 California Institute of Technology. Government sponsorship acknowledged

INTRODUCTION

The Mars Science Laboratory (MSL) mission landed a 900 kg rover, the heaviest payload landed on Mars to date. The next NASA flagship mission to Mars, Mars 2020, plans to land a payload of ~ 1050 kg using the same lander architecture and technology as MSL. The ~ 150 kg increase in landed payload mass is made possible by the greater atmospheric density at the time of landing compared to MSL. The heritage technology and architecture used by MSL and Mars 2020 largely was qualified in the Viking era and is generally acknowledged as nearing its limits ¹.

A Sample Return Lander (SRL) is a candidate for the next NASA Mars mission after Mars 2020. Over the past several years, payloads of various sizes and masses have been studied for the candidate SRL mission, many of which are heavier than the Mars 2020 payload ^{2,3}. It is likely that a future SRL mission would require some changes to the Viking-era technology to land increased payload masses. The upper end of the range of payload mass could pose a challenge for the MSL-class, parachute-based architecture.

The use of Supersonic Retropropulsion (SRP) instead of a parachute is almost certain for future large human-class missions with entry masses in the tens of metric tons, because of the limits of parachute systems ^{4,5,6}. The use of SRP has also been discussed for robotic missions in the SRL class ^{2,7}. We explore in this paper various aspects of EDL performance using SRP, and propose a notional configuration for an SRP lander for an SRL - class mission.

One important metric for EDL performance is Propellant Mass Fraction (PMF), which we define here as (propellant mass at descent engine ignition) / (total wet lander mass at descent engine ignition). PMF is “scalable”: two vehicles with the same thrust-to-weight ratio (T/W), specific impulse (Isp), powered descent guidance algorithm, and position and velocity from the target at ignition have the same PMF requirement to land at the target.

With SRP, the propellant requirement is higher than it is with the chute-based architecture since additional propellant is needed to compensate for lack of drag from the chute. However SRP frees the vehicle from parachute deployment constraints. Deployment of a parachute should occur within a qualification region of dynamic pressure and Mach number, and also at an altitude high enough above the landing site to provide enough time to accomplish activities required to slow for touchdown. An example illustration of this supersonic chute deployment region (the “Mach-Q box”) is shown in Figure 1, taken from reference 1.

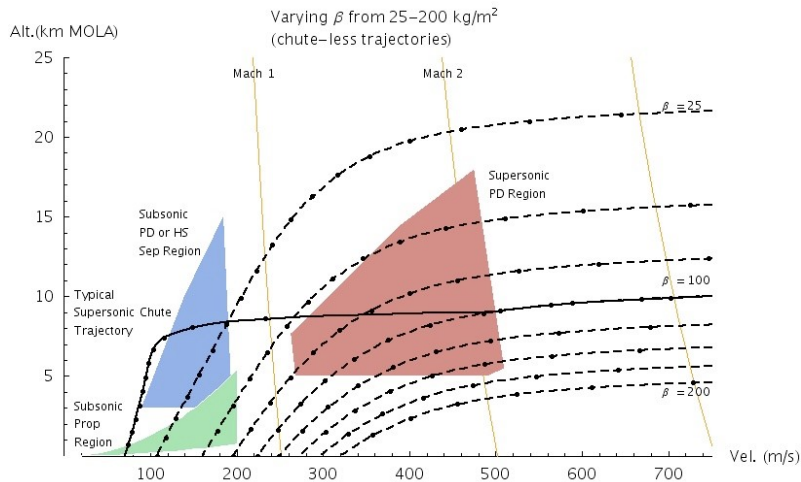


Figure 1: Increasing ballistic coefficient from 25 – 200 kg/m². For ballistic coefficient $> \sim 150$ kg/m², trajectories fall below the Viking-heritage supersonic parachute deployment region

In this figure, the left bound of the Mach-Q box is a lower Mach limit of 1.1, the right bound is an upper Mach limit of 2.1, the top of the box is a 250 Pa lower limit on dynamic pressure, and the lower right corner is a 1200 Pa upper limit on dynamic pressure. The bottom of the box is a lower altitude limit shown at 5km above the surface, which can be considered “slightly aggressive”.

For the chute-based architecture, as landed payload mass increases, entry mass and entry ballistic coefficient also increase until it is no longer possible to deploy the parachute within qualification limits while meeting timeline constraints. In the example shown in the figure, the trajectory does not enter the Mach-Q box at all for entry ballistic coefficients $> \sim 175 \text{ kg/m}^2$. (For comparison, MSL’s entry ballistic coefficient was $\sim 135 \text{ kg/m}^2$; Mars 2020’s is 143 kg/m^2). The figure shows the landing site elevation at 0 MOLA (w.r.t. the Mars Orbiter Laser Altimeter reference surface). It is possible to lower the altitude-imposed lower limit of the Mach-Q box by reducing landing site elevation below 0 MOLA, allowing deployment inside the Mach-Q box for higher entry ballistic coefficients. However a practical limit on entry ballistic coefficient of perhaps 200 kg/m^2 is imposed by the surface of Mars and the landing site elevations at which scientifically attractive targets are found. The Mars Science Laboratory mission landed at an elevation of -3.4 km MOLA . The highest site elevation under consideration for the Mars 2020 mission is $\sim 2 \text{ km}$ ⁸.

With SRP, it is possible to safely land a vehicle with an entry ballistic coefficient of up to 600 kg/m^2 ^{2 4 7}. SRP makes it possible to increase entry ballistic coefficient and entry mass enough to be able to carry all the additional propellant and other mass that is needed and also to increase landed payload mass. Lobbia, Wolf, and Whetsel² showed that as entry ballistic coefficient is increased, the fuel-optimal ignition speed increases, and consequently the PMF requirement increases as well. Figure 2, reproduced from the reference, shows the variation.

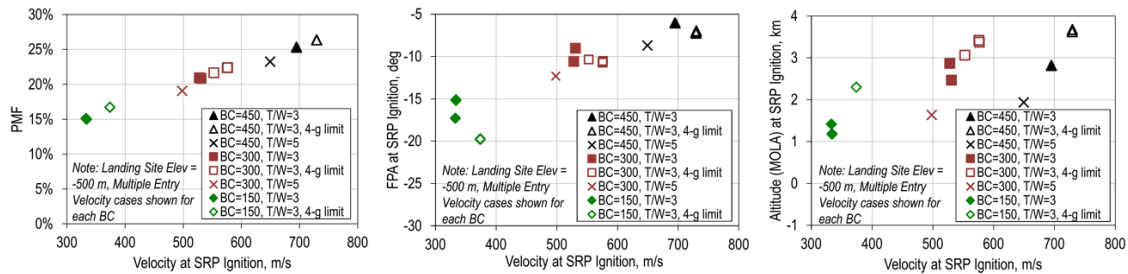


Figure 2: Performance sensitivities to SRP ignition velocity ²

PROPELLANT REQUIREMENT UNDER DISPERSIONS: MONTE CARLO STUDY

The results shown in Figure 2 were generated for nominal trajectories only and do not include the effects of uncertainties on various parameters important to EDL. A preliminary Monte Carlo study was undertaken as part of this work to investigate the effect of dispersing selected input parameters on the propellant requirement. Inputs dispersed were entry states, atmospheric density, uncertainties in 6DOF aerodynamic coefficients, and uncertainty in the center of mass.

In addition, we were interested in comparing the performance of the legacy “bank control” architecture used on Gemini, Apollo, and MSL to an alternative architecture using flaps for aerodynamic control during entry.

In the bank-control architecture, an offset center of mass creates an angle of attack and a lift vector. The direction of the lift vector is controlled by banking the spacecraft with Reaction Con-

trol System (RCS) thrusters. The Apollo guidance algorithm⁹ calculates the desired vertical component of the lift-to-drag ratio as a function of range to go to the target and converts that to a commanded bank angle. This architecture has important advantages including simplicity of both guidance and control.

However there are also disadvantages to the bank control architecture which motivate investigation of other options. Bank control requires the use of bank reversals to stay within an entry corridor. During bank reversals, which can consume ~10-20% of the duration of the entry trajectory, no control of downrange distance to the target is possible. Range error grows significantly during bank reversals, and can be reduced to pre-reversal levels only with sufficient time-to-go to the target.

Cianciolo & Powell⁴ discussed various alternative architectures for “Direct Force Control” for large, human-class missions including incorporation of a moving mass to control the center of gravity in flight, modulating the shape of an inflatable forebody, inflating or deflating a flap, using an asymmetric deployable device, or adding aerodynamic flaps to modulate angle of attack (AoA) and sideslip angle. Cianciolo and Powell explored performance of an entry vehicle with flaps in a configuration proposed by Korzun, Dutta, and Cianciolo⁵ illustrated in Figure 3 (taken from the reference). The vertical flaps in the figure (labeled α) are used to modulate angle of attack, and the horizontal flaps in the figure (labeled β) are used to modulate side force as needed for heading / sideslip control. They showed that aerodynamic flaps can be used to deliver the vehicle more accurately to a point at which a gravity-turn powered descent can be initiated, reducing propellant consumption dispersions. Cianciolo and Powell allowed engine thrust to be modulated between 75% and 85%.

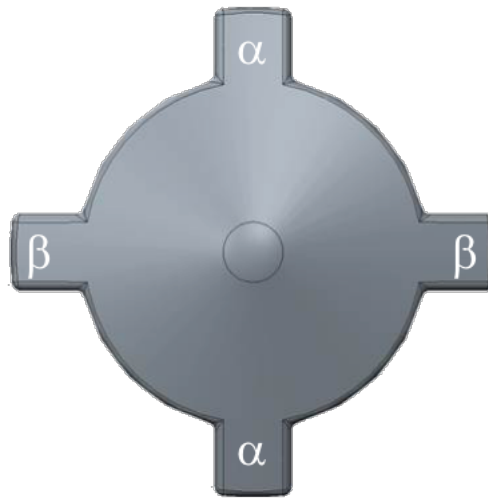


Figure 3: Vehicle configuration with four aerodynamic control surfaces proposed by Korzun, Dutta, and Cianciolo⁵

Flapped vehicle entry guidance and control

The area of each flap was assumed to be 6% of the vehicle reference area without flaps. Flap aerodynamics coefficients are described in Korzun, Murphy, and Edquist¹⁰, and were applied as “deltas” to the aerodynamic database for a 70-deg sphere cone.

For simplicity, Apollo entry guidance was adapted for use with flaps. The “vertical” flaps in Figure 3 modulate AoA to achieve the desired vertical component of the lift to drag ratio calculated by Apollo guidance, instead of banking the vehicle to achieve the desired vertical L/D com-

ponent as is done in the bank-control architecture. The “lateral” flaps in Figure 3 control cross-range; consequently there is no need for bank reversals.

Apollo entry guidance commands vertical L/D, the ratio of the lift and drag coefficients

$$Cl/Cd = (L/D)_{\text{vertical}}$$

The lateral acceleration command is proportional to heading error and current available lift:

$$A_{\text{side}} = K * L * \Delta\psi$$

From A_{side} , an estimate of the desired side force coefficient can be obtained

$$C_y = A_{\text{side}}/qS$$

where q is dynamic pressure and S is the reference surface area.

A 2D search is performed in the combined aerodatabase (70-deg sphere cone + flap deflection “deltas”) to find the vertical and horizontal tab deflections dv and dh that provide both Cl/Cd and C_y

When flaps are used, uncertainties in the position of the center of mass induce nonzero bank angles, which compromise the effectiveness of the flap control system leading to large crossrange errors. To remedy this, a PD (proportional – derivative) bank control model with applied torque was added to emulate an RCS thruster model. Constraining bank angle to within a ± 5 degree deadband kept the maximum crossrange errors within 2 km. The amount of additional propellant required to control the bank angle deadband was estimated in a Monte Carlo simulation to be < 5.0 kg.

PID (proportional-integral-derivative) gains are applied to both α and β channels to reduce L/D and side slip errors. L/D and side-slip commands are converted to flap deflection commands. L/D gains are adjusted to match commanded the vertical L/D profile. Side slip gains are adjusted to remove cross-track errors.

A deflection rate limit is imposed on the flaps. This was optimized for stability in α and β . The α flap limit used was 140 deg/s; the β flap limit was 33 deg/s. A 20 deg range of motion was assumed for the flaps. The scope of this work did not include design trades on flap actuators or other vehicle elements to establish realistic limits on flap deflection or rates.

Bank-control vehicle: entry control

A PD controller is used to apply bank angles commanded by Apollo guidance. RCS thrust control is simulated with an external torque applied directly to the s/c about the velocity vector (bank axis). A limit of 20 deg/sec is imposed on bank rate, and a limit of 5 deg/sec² is imposed on bank acceleration.

Powered descent

For this work, propellant-optimal powered descent guidance was implemented in conjunction with deeper engine throttling, for both bank control and flapped vehicle architectures. Simulations were created incorporating the G-FOLD (Guidance for Optimal Large Diverts) powered descent guidance algorithm ¹¹, for both a bank-control vehicle and a vehicle with flaps in the configuration of Figure 3. Given initial conditions at ignition (position and velocity vectors relative to the target and relevant spacecraft parameters (wet mass at ignition, thrust-to-weight ratio, thruster Isp and descent engine cant angles if the engines are canted), G-FOLD computes a ΔV -optimal trajectory to the target.

Triggering engine ignition

To minimize propellant consumption, it is necessary not only to compute a propellant-optimal trajectory to the target as G-FOLD does, but also to be able to choose the optimal descent engine ignition point on the entry trajectory. To accomplish this, our simulation uses G-FOLD to compute the optimal powered descent trajectory to the target at each time point on the entry trajectory after the spacecraft slows to a threshold speed of 850-900 m/s. When G-FOLD's computed propellant consumption increases beyond a specified propellant mass threshold (instead of decreasing), ignition is triggered.

While useful in our simulations, this approach is probably too computationally intensive to be effective onboard a spacecraft. A table lookup method for triggering ignition has been shown to be feasible in a Matlab prototype but was not implemented in the present Monte Carlo simulation study. In this method, a table is created from which it is possible to extract the propellant required to land at the target from a range of ignition conditions (speed, flight path angle, altitude, and distance from the target)¹⁸. This table can be queried at each time point on the trajectory to determine when to trigger ignition instead of running G-FOLD onboard at each time point as described above.

The assumed engine throttling limit was 50% thrust for both flapped and bank-control vehicles. If engines cannot be throttled down as far as 50% thrust, a solution could be to shut down some engines in lieu of throttling all the engines at the same time. If engines that are shut down cannot be quickly restarted, the thrust may not be able to follow the "bang-off-bang" profiles which are generally optimal, in which case there could be a propellant mass penalty for shutting down some engines early.

Other assumptions

Table 1 summarizes modeling methodology used in the simulation for both bank-control and flapped vehicles. Selected Monte Carlo assumptions / inputs are tabulated in Table 2.

Table 1: Modeling used for simulations of bank-control and flapped vehicles

	ROLL-CONTROL VEHICLE	FLAP-EQUIPPED VEHICLE
Entry phase		
Guidance	Apollo entry guidance (generates bank angle commands)	Modified Apollo entry guidance (generates flap deflection commands)
Control	Bank angle changes to follow guidance commands, torque applied to s/c specified as function of commanded bank (no thruster firings modeled)	Flap deflections to follow guidance commands, with flap motion at hypothetical rate & acceleration.
Body dynamics / forces	Lift and drag vectors calculated from 6dof aerodatabase	Lift and drag vectors calculated from 6dof aerodatabase + "delta" aerodatabase for flaps
Knowledge sensing	no sensors modeled ("perfect knowledge")	no sensors modeled ("perfect knowledge")
Powered descent phase		
Guidance	G-FOLD generates required thrust magnitude and direction	G-FOLD generates required thrust magnitude and direction
Control	Exactly follows commands prescribed by powered descent guidance	Exactly follows commands prescribed by powered descent guidance
Body dynamics / forces	Thrust vector fixed in body coords, no aero lift or drag modeled	Thrust vector fixed in body coords, no aero lift or drag modeled
Knowledge sensing	no sensors modeled ("perfect knowledge")	no sensors modeled ("perfect knowledge")

Table 2: Selected Monte Carlo assumptions for both bank-control and flapped vehicles

Parameter	Units	Value
Mars arrival Ls	deg	150
Inertial entry speed	km/s	6.5
Nominal Atm dusttau		0.48
Landing site elevation	m	-500
Targeted vert spd at ldg	m/s	0.75
Aeroshell diameter	m	4.7
Entry ballistic coefficient	kg/m ²	450
L/D at entry		0.24
Entry mass	kg	11440
Propellant Isp	sec	295
T/W at ignition		3

A single in-plane trajectory was used as the reference trajectory for Apollo guidance for both vehicles. The same set dispersed entry states was used for both. The MarsGRAM atmospheric model was used for both, with mean dusttau=0.48, minimum 0.1, and maximum 1.0. The arrival Ls at Mars was 150 deg., corresponding to the lowest-density atmosphere in the Martian atmospheric pressure cycle and consequently a “worst-case” for EDL performance. All cases were targeted to achieve a vertical velocity of 0.75 m/s at the nominal landing site in G-FOLD.

Entry ballistic coefficient was 450 kg/m² (entry mass 11440 kg) for this Monte Carlo study. This value was chosen as a stressing case to explore feasibility of flying trajectories at high ballistic coefficients. This is not representative of any existing vehicle design concept, which would require packing densities significantly higher than flown on previous robotic missions. We describe a vehicle concept in a following section with a ballistic coefficient of 267 kg/m².

Aerodynamic drag was not modeled after engine ignition. Experimental results have found that there is little or no aerodynamic drag contribution during SRP¹². This is a conservative assumption for estimating propellant consumption because the presence of aerodynamic drag reduces propellant consumption.

“Perfect onboard state knowledge” was assumed.

Results

Monte Carlo results are shown in Figures 4 and 5 on the following pages. Dispersions of velocity and altitude at ignition are larger for the bank-control vehicle than for the vehicle with flaps, leading to larger dispersions in propellant consumption for the bank-control vehicle as well. All trajectories landed within 20m of the target. Feedback gains were applied to accelerations in G-FOLD to aid targeting. The “non-Gaussian” appearance of the propellant consumption dispersions in the downrange direction is an artifact of the stronger gain in the downrange direction. We believe “tuning” can alter this if needed.

The 99.87% propellant consumed is 26.9% PMF / 3082 kg for the bank-control vehicle, and 25.1% PMF / 2878 kg for the flapped vehicle, producing a savings in entry mass of 1.8% PMF / 204 kg for the flapped vehicle. This propellant mass savings is offset by the mass of the four flaps (including thermal protection) and associated actuator hardware. Although a detailed estimate of the flap system was not done as part of this work, it seems unlikely that this trade produces a significant net savings in entry mass for the flap system, for a robotic lander of the class considered here (entry mass of several thousand kg).

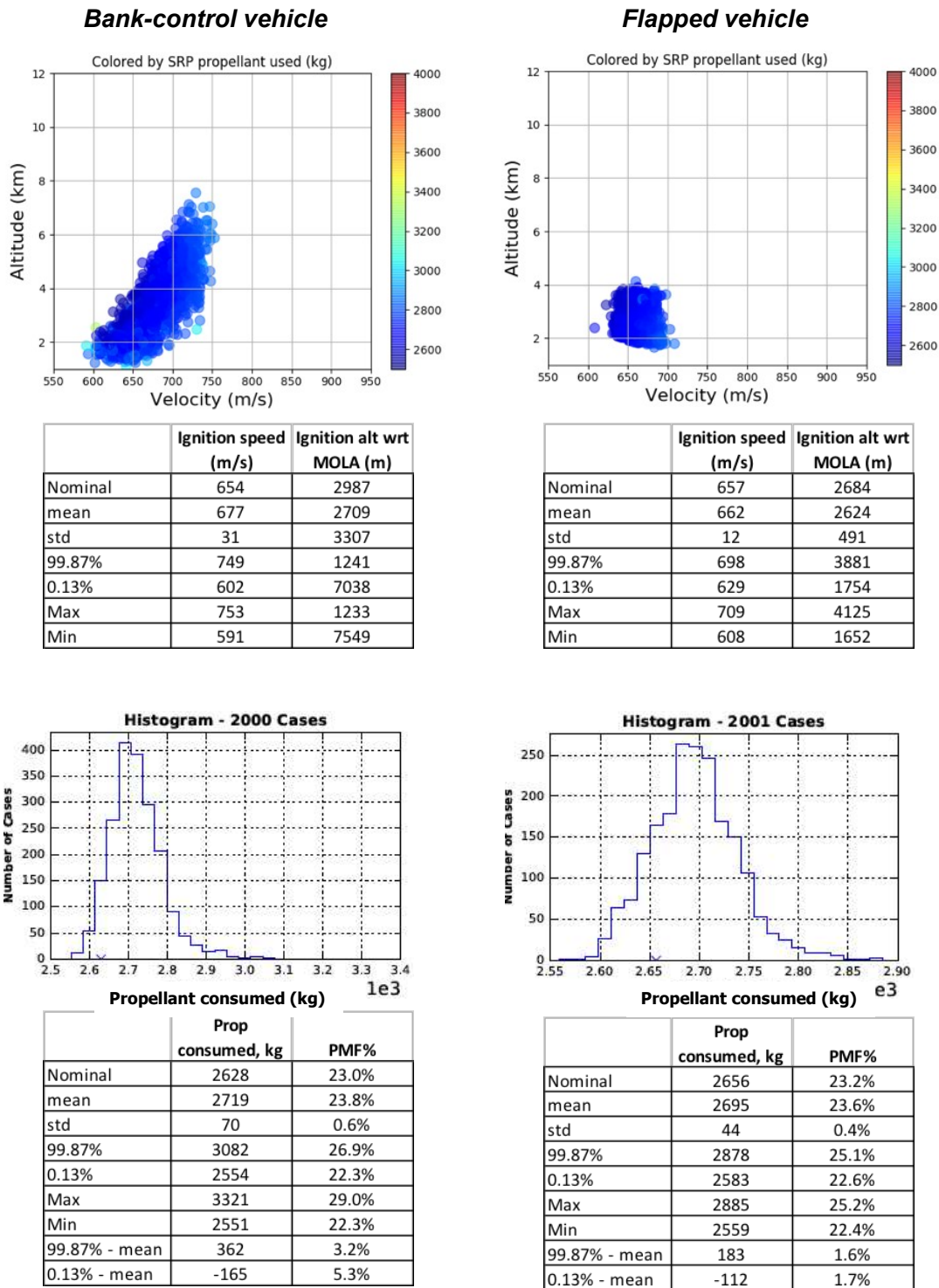
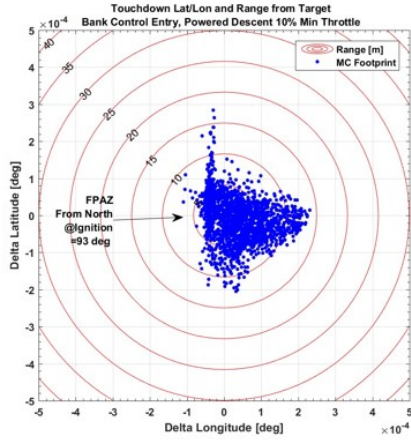
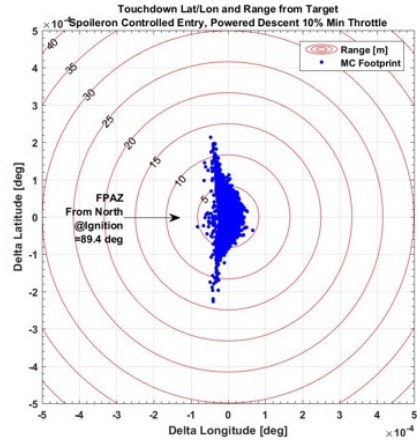


Figure 4: Monte Carlo results: propellant consumption, ignition speed, and ignition altitude

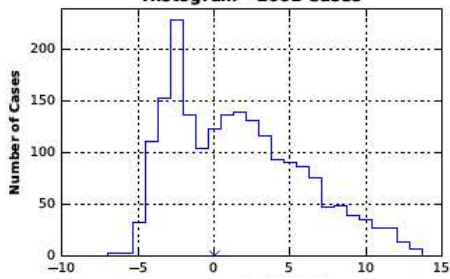
Bank-control vehicle



Flapped vehicle

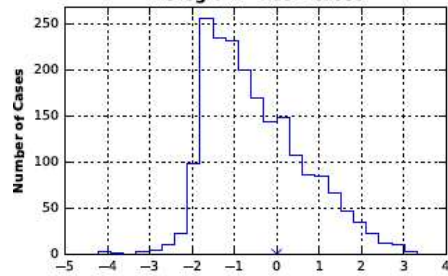


Histogram - 2001 Cases



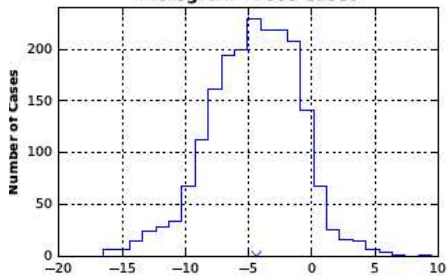
Downrange dist at touchdown (m)

Histogram - 2001 Cases



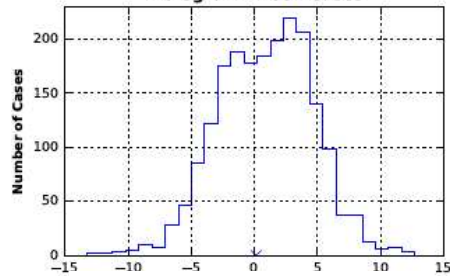
Downrange dist at touchdown (m)

Histogram - 2000 Cases



Crossrange dist at touchdown (m)

Histogram - 2001 Cases



Crossrange dist at touchdown (m)

	Downrange dist at ldg (m)	Crossrange dist at ldg (m)
Nominal	0.00	0.00
mean	1.63	-4.56
std	4.27	3.57
99.87%	13.23	6.90
0.13%	-5.87	-15.96
Max	13.74	9.49
Min	-7.00	-16.52

	Downrange dist at ldg (m)	Crossrange dist at ldg (m)
Nominal	0.00	0.00
mean	-0.49	0.91
std	1.14	3.71
99.87%	2.93	11.70
0.13%	-3.95	-11.47
Max	3.32	12.72
Min	-4.24	-13.32

Figure 5: Monte Carlo results: landing accuracy

POTENTIAL BENEFITS OF USING FLAPS FOR DRAG MODULATION

It is also possible to modulate drag by commanding all four flaps to move collectively in and out to adjust for density variation. With sufficient control authority, drag modulation can prevent velocity from deviating from the reference trajectory. Drag modulation was not implemented in our simulation, however a preliminary analysis using optimal control was performed to attempt to quantify the potential propellant savings which could be realized by using the flaps to modulate drag through changes in aerodynamic reference area in addition to L/D and side force via AoA and sideslip angle modulation.

In this analysis, as a proxy for modulation of drag with flaps, ballistic coefficient was modulated by increasing vehicle area in the simulation while maintaining a constant hypersonic drag coefficient. Lift was modulated by varying L/D. Trajectories were optimized to minimize propellant consumption. Results are shown in Figure 6. Three strategies were investigated: minimum ballistic coefficient (flaps always fully deployed, labeled “flaps out” in Figure 6), variable ballistic coefficient (optimizer chooses when to deploy flaps, labeled “actuated” in Figure 6), and maximum ballistic coefficient (flaps never deployed, labeled “flaps in” in Figure 6).

The results show that a single step change in ballistic coefficient from high to low is PMF optimal. Further, reducing ballistic coefficient through flap deployment at the proper time reduces the required propellant load for SRP. With 24% flap area fraction (the total of assumed in the above Monte Carlo study with four flaps of 6% area fraction each, illustrated with colored stars in the figure), the PMF savings with “flaps out” is ~1.6% (from 16% down to 14.4%); if ballistic coefficient is allowed to vary (flaps “actuated”), PMS savings are approximately 2.2% (from 16% down to 13.8%). This is close to the 1.8% PMF savings that the above Monte Carlo results show from using flaps for AoA modulation only.

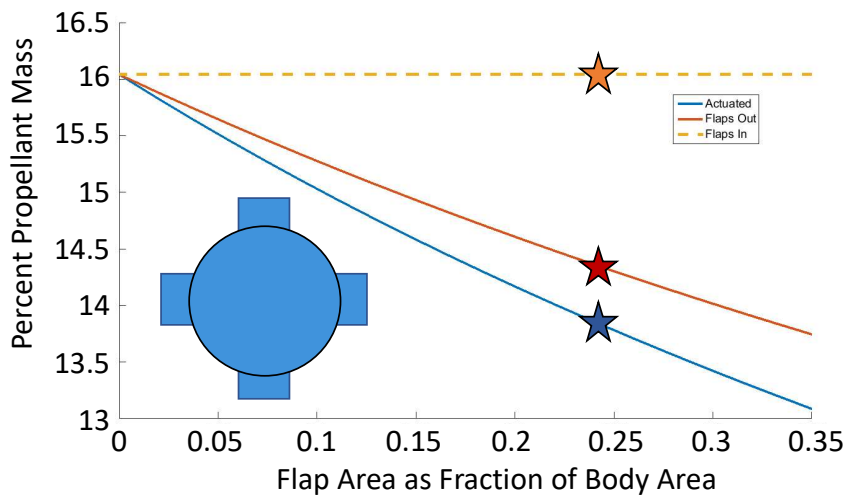


Figure 6: Predicted PMF savings from use of flaps for drag modulation

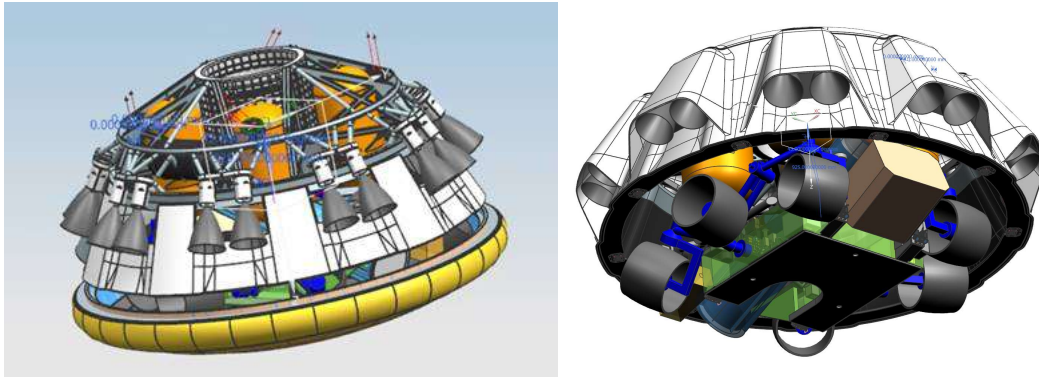
However, in a more realistic mission scenario where flaps are used to modulate angle of attack and sideslip, a reduced amount of flap control authority would be available for drag modulation. Therefore, larger flap areas are likely required to achieve the PMF reduction benefit shown in Figure 6 on a flight system.

SIZING AND CONFIGURATION FOR SAMPLE RETURN LANDER-CLASS MISSION

One challenge associated with SRP is the lack of a parachute to slow the lander after heatshield separation so that the heatshield can fall away after separation. Consequently SRP configurations have been proposed in which the heatshield is not jettisoned but stays with the vehicle until touchdown. In the configuration discussed by Lobbia, Wolf, and Whetsel ², the backshell and heatshield both remain with the lander until touchdown. Jettisoning the heatshield is helpful however, since the presence of the heatshield after touchdown complicates egress of a rover, and also requires SRP engines to fire through the heatshield during powered descent.

To facilitate jettisoning the heatshield, we propose here a configuration which is a variation of the “skycrane” used on MSL. However instead of mounting the descent engines on a stage inside the backshell, the backshell itself is used as the descent stage, with engines integrally mounted on the backshell. We developed an example concept for a bank-control SRP lander along these lines, shown in Figure 7. Although aerodynamic drag may be minimal once the SRP engines are ignited, the heatshield is expected to experience significant drag soon after separation as it travels beyond the boundary of the aerodynamic shock. Therefore in order to prevent the lander from re-contacting the jettisoned heatshield, jettison should be delayed until the drag acceleration that the heatshield would experience outside the shock region is less than the acceleration that the rest of the lander experiences under thrust from the SRP engines. On example trajectories we looked at, this occurs at altitudes of a few hundred meters. Heatshield avoidance would be assured with a small divert maneuver, similar to the 300m backshell avoidance maneuver performed during powered descent on MSL. (This was not included in our analysis of propellant requirement and would require a small increase in the propellant budget.)

Figure 7: Lander configuration concept with descent engines mounted on the backshell



Descent engines

Aerojet R-40 bipropellant engines were selected for our vehicle concept. These served as the RCS engines on Shuttle. The R-40 was rated at 4000 N thrust, and had an Isp of 281 sec with Shuttle nozzle configurations which were not optimized for maximum thrust. A custom R-40 engine with the Shuttle injector and chamber and a custom scarf nozzle (shaped for integration into our aeroshell) could deliver an estimated maximum thrust of 5460N at an Isp of 293 sec. Engines

are assumed to be canted at a 30 deg angle from the roll axis of the lander in concert with their mounting on the backshell. An effective Isp is derived from multiplying Isp by the cosine of the engine cant angle and a factor of 0.985 to account for plume loss. Effective Isp for this engine is then 250 sec.

The R-40 has been successfully tested down to 58% of maximum thrust during ground testing, but was not throttled on-orbit. The development of a new throttle valve for onboard use (at modest cost) to control the propellant flow rates would enable throttling down to ~60% with the objective of throttling to 50% thrust.

Sizing

In sizing a notional SRP lander for an SRL (Sample Return Lander) mission, we assumed a landed payload mass of 1300 kg. which we believe is at the higher end of the likely SRL payload mass range and could also be a challenge for the chute-based architecture. As landed payload mass increases, more enhancements must be made to the chute-based architecture to keep it viable. SRP requires significantly greater entry mass (and therefore launch mass), but becomes a more attractive option as the cost and complexity of those enhancements increases. There is probably a “transition region” in landed payload mass in which SRP and chute-based architectures compete. If so, our 1300 kg landed payload mass is probably in this transition range.

Sizing the lander was an iterative process involving refinement of an initial guess. The starting point was an initial guess of entry ballistic coefficient of ~250 kg/m² which sized the PMF requirement at ~25% (~22% nominal from Figure 2 + ~3% for dispersions from Figure 4). Assuming a 4.7m diameter aeroshell, the corresponding entry mass is ~6355 kg. This initial estimate of entry mass was used to size structural mass components.

Using the R-40’s effective Isp of 250 sec, maximum thrust of 5460N per thruster, and assuming a T/W of 3 at ignition (consistent with the assumptions used to construct Figure 2), we find that the maximum wet mass at ignition is 7133 kg with 16 engines or 7985 kg with 18 engines. We chose 18 engines to provide generous growth margin to maintain a T/W of 3 or greater.

A mass breakdown, shown in Table 3, was constructed for all components of entry mass for the proposed bank-control SRP lander based on the rough initial guesses of parameters above.

Table 3. Mass breakdown for a notional SRP lander

	Mass estimate, kg (includes growth contingency)	Comments
Launch mass	7860.33	
Cruise Stage	789.00	structural mass scales with entry mass
Cruise Balance Mass	283.48	scales with entry mass
Entry mass	6787.85	
Entry Balance Mass	318.13	scales with entry mass
Wet mass at ignition	6469.72	
Avionics	75.84	
GN&C	39.03	
Telecom	36.80	
Thermal	34.35	
Harness	38.18	
Propulsion (dry mass)	734.85	
Mechanical	1264.80	scales with payload, portions estimated from CAD
Propellant	1617.43	25% PMF
Heatshield	1328.44	jettisoned at several hundred m alt prior to ldg
Payload	1300.00	

Masses were estimated by scaling subsystems from MSL/M2020’s descent stage, performing bottom-up estimates for the heatshield and other selected components, and calculations from rough CAD configuration models of the upper structure. Estimated entry mass is 6787 kg, and estimated ballistic coefficient is 267 kg/m².

Launch mass includes the mass of a cruise stage. In addition, for an SRP bank-control vehicle a cruise balance mass is included in launch mass, following the MSL / Mars 2020 paradigm in which the spacecraft is spin-stabilized in cruise but flies a 3-axis stabilized atmospheric entry with an offset center of mass. The entry balance mass is jettisoned prior to entry and is not included in entry mass.

For an SRP flapped vehicle, the center of mass is not offset during entry; consequently no cruise balance mass is needed. This reduces launch mass, but not entry mass, for the flapped vehicle.

MSL also carried entry balance mass, which was jettisoned just prior to parachute deployment to remove the center-of-mass offset (referred to as “Straighten Up and Fly Right” or SUFR), allowing the parachute to deploy at a nominal AoA of 0 deg. in order to ensure successful deployment and avoid large angular rates during deployment¹³. For a flapped vehicle with SRP, this is not needed since it has no parachute, and since the center of mass is not offset during entry. For a bank-control SRP lander with an offset center of mass during entry, eliminating the entry balance mass has the consequence of requiring the lander to fly with an offset center of mass during powered descent. Our work did not include investigation of the controllability of the lander or sizing of the propulsion system with an offset center of mass, so we have retained an entry balance mass in our bank-control vehicle concept as shown in the mass breakdown. However, eliminating it is a credible option which should be investigated in future work and which could produce significant entry mass savings. These entry and cruise balance mass options are summarized in Table 4.

As Table 5 shows, our estimate of launch mass of 7860 kg is within the capability of the Delta IV Heavy or Falcon Heavy (expendable) launch vehicles for minimum-C3 launches in either 2026 or 2028, with large margins to accommodate either mass growth or increases in launch C3 that may result from more judicious selection of launch / arrival dates. It may be possible to eliminate the entry balance mass as discussed above, providing additional margin.

Table 4. Cruise and Entry balance mass requirements

<i>Balance masses required?</i>	Chute-based architecture?	SRP bank-control vehicle?	SRP flapped vehicle?
Cruise balance mass	Y	Y	N
Entry balance mass	Y	(?)	N

Table 5. Minimum-C3 launch vehicle capabilities for 2026 and 2028 opportunities¹⁴

	2026 opportunity:	2028 opportunity
	C3=9.14 km²/s²	C3=8.93 km²/s²
Falcon Heavy (expendable)	10075	10130
Delta IV H (NLS II)	8600	9040
Atlas V 551	5150	5170

CONCLUSIONS

An SRP architecture is unconstrained by the need to deploy a parachute within the required “Mach-Q box” to assure successful parachute inflation. Consequently, significantly higher entry ballistic coefficients are feasible with SRP than with parachutes. Although more propellant and a heavier propulsion system are required for SRP, ability to increase entry mass enables heavier landed payload mass.

Propellant consumption dispersions are reduced with the use of aerodynamic flaps for AoA modulation only, producing savings of ~1.8 PMF% (~200 kg for a vehicle with entry mass of 11440 kg and a 4.7m-diameter aeroshell). This savings is offset by the added mass of the flap system hardware including surfaces and actuators, which could reduce or eliminate the propellant mass savings. However, a preliminary analysis indicates that additional propellant savings of up to the same magnitude may result with the use of flaps for drag modulation as well as AoA modulation. In addition, a flapped vehicle requires no cruise balance mass (producing savings in launch mass but not entry mass), and no entry balance mass (producing savings in both). Entry balance mass may not be needed for an SRP bank-control vehicle either; however eliminating it requires the vehicle to be controllable during powered descent with an offset center of mass.

Developing a guidance algorithm for use with AoA and drag modulation with flaps and testing it in simulations, developing a detailed mass estimate for the flap system hardware, and investigating the controllability of the lander during powered descent with an offset center of mass are recommended for more accurately assessing the potential for mass savings with a flapped vehicle compared to a bank-control vehicle.

A preliminary vehicle concept has been developed to land a payload of 1300 kg with SRP. Estimated launch mass for this vehicle is 7860 kg, within the capability of the Delta IV Heavy or Falcon Heavy (expendable) launch vehicles. With the configuration described here using the backshell as an “skycrane” it is possible to jettison the heatshield at an altitude of several hundred meters above the surface, allowing a rover payload to land on its wheels as the MSL Curiosity rover did. A maneuver after jettisoning the heatshield is recommended to avoid heatshield recontact.

Future crewed missions are expected to have little in common with current robotic EDL systems and would likely rely on SRP. Use of SRP on a robotic mission like a notional Mars Sample Return Lander could be a useful technology development step. A science mission like SRL could pose an opportunity for a demonstration of SRP that would feed forward to future crewed missions.

ACKNOWLEDGMENTS

The authors would like to acknowledge the advice and support of Chad Edwards and Charles Whetsel throughout the course of this work. This research was carried out at the Jet Propulsion Laboratory, California Institute of Technology, under a contract with the National Aeronautics and Space Administration.

REFERENCES

- ¹ R.D Braun and R. M. Manning, "Mars Exploration Entry, Descent, and Landing Challenges." *Journal of Spacecraft and Rockets*. Vol. 44, No. 4, 2007, pp. 310-323.
- ² Lobbia, M., Wolf, A., Whetsel, C., "Supersonic Retro-Propulsion for Future High-Mass Robotic Mars Lander Missions," *ISTS Conference 2017*
- ³ Klein, E., Nilsen, E., Nicholas, A., Whetsel, C., Parrish, J., Mattingly, R., May L., "The Mobile MAV concept for Mars Sample Return," IEEE Aerospace Conference, Big Sky, MT, 1-8 March, 2014
- ⁴ Dwyer Cianciolo, A., Powell, R.W. "Entry, Descent, and Landing Guidance and Control Approaches to Satisfy Mars Human Mission Landing Criteria," AAS Paper 17-254, 27th AAS/AIAA Space Flight Mechanics Meeting; 5-9 Feb. 2017; San Antonio, TX
- ⁵ Korzun, A., Dutta, S., Dwyer Cianciolo, A., "Blunt Body EDL System Performance Improvements Through Direct Force Control and Deployable Tabs," presentation at the 14th International Planetary Probe Workshop, 12-16 June, 2017, The Hague, Netherlands
- ⁶ Price, H., Manning, R., Sklyanskiy, E., and Braun, R.: A High-Heritage Blunt-Body Entry, Descent, and Landing Concept for Human Mars Exploration, AIAA Paper 2016-0129, 2016 AIAA Science and Technology Forum and Exposition, San Diego, CA, January 2016.
- ⁷ Noyes, C., Wolf, A., and Benito, J., "High Ballistic Coefficient Mars EDL With Supersonic Retropropulsion," AAS Paper 17-034 (2017).
- ⁸ <https://marsnext.jpl.nasa.gov>
- ⁹ Carman, G.L., Ives, D.G., and Geller, D.K., "Apollo-Derived Mars Precision Lander Guidance," Paper 1998-4570, 23rd Atmospheric Flight Mechanics Conference, 10-12 August, 1998, Boston, MA
- ¹⁰ Korzun, A.M., Murphy, K.J., Edquist, K.T., "Supersonic Aerodynamic Characteristics of Blunt Body Trim Tab Configurations," paper AIAA-2013-2809, 31st AIAA Applied Aerodynamics Conference, 24-27 June, 2013, San Diego, CA
- ¹¹ B. Acikmese and S. Ploen, "Convex Programming Approach to Powered Descent Guidance for Mars Landing." *AIAA Journal of Guidance, Control, and Dynamics*. Vol. 30, No. 5, 2007, pp. 1353-1366.
- ¹² Korzun, A.M., Braun, R.D., and Cruz, J.R., "Survey of Supersonic Retropropulsion Technology for Mars Entry, Descent, and Landing," *Journal of Spacecraft and Rockets*. Vol. 46, No. 5, 2009, pp. 929-937
- ¹³ Stelzner, A.D., San Martin, M., Rivellini, T.P., Chen, A., and Kipp, D., "Mars Science Laboratory Entry, Descent, and Landing System Development Challenges," *Journal of Spacecraft and Rockets*. Vol. 51, No. 4, 2014, pp. 994-1003
- ¹⁴ <https://elvperf.ksc.nasa.gov>
- ¹⁵ Lorenz, C.G., and Putnam, Z.R., "Optimal Hypersonic Trajectory Strategies for Supersonic Retropropulsion at Mars," AIAA Atmospheric Flight Mechanics Conference, Grapevine, TX, 9-13 January, 2017
- ¹⁶ Wolf, A., Casoliva, J., Benito, J., Acikmese, B., Ploen, S., "Improving the landing precision of an MSL-class vehicle," IEEE Aerospace Conference, Big Sky, MT, 3-10 March, 2012
- ¹⁷ Post, E., Dupzyk, I., Dyakonov, A., Korzun, A., Tanimoto, R., Edquist, K., "Supersonic Retropropulsion Flight Test Concepts," 8th International Planetary Probe Workshop, 6-10 Jun. 2011, Portsmouth, VA
- ¹⁸ Scharf, D.P. and Ploen, S.R., "Interpolation-Enhanced Powered Descent Guidance for Onboard Nominal, Off-Nominal, and Multi-X Scenarios," paper AIAA 2015-0850, AIAA Guidance, Navigation, and Control Conference, 5 – 9 January, 2015, Kissimmee, FL